Additive Manufacturing of Stretchable Piezo-Resistive Sensors: Fabrication and Performance Evaluation

A Thesis Submitted to

The University of Texas at Arlington

by

Mohammad Ahnaf Shahriar

(ID: 1001837256)

In partial fulfillment of the requirements for the degree of

Master of Science, Industrial Engineering

December 2022

Department of Industrial, Manufacturing, and Systems Engineering

Dissertation Committee:
Committee Chair: Dr. Emma Yang
Committee Members: Dr. Yi Hong, Dr. Shuchi Deb, Dr. Xin Liu

Acknowledgments

I would like to start by thanking Dr. Emma Yang, my thesis committee chair and supervisor. I feel incredibly fortunate and indebted to have had the chance to work with her. Without her assistance and regular direction, it would be impossible to complete the thesis in such a short amount of time. Thanks to her guidance, I could complete my experiment work and writing. I would want to extend my sincerest gratitude to her.

I want to thank everyone on my committee. I feel honored to be in their company. I want to express my sincere thanks to Dr. Hong for letting me conduct a portion of my experiment countless times at his laboratory. I would want to convey my gratitude to Dr. Deb, who is my course instructor and has been very helpful. I want to express my thankfulness to Dr. Liu for his presence.

I want to say thank you to Kobir. Throughout the year, he has been a huge assistance. Being a novice in the research field has been a challenge for me. He has always been there for me whenever I needed assistance of any type. Lei also deserves my gratitude. He provided me with the training when I first began working in the SIGMA lab, and that training served as a crucial foundation for me.

Lastly, I want to thank the department of Industrial, Manufacturing, and Systems Engineering (IMSE). It has been a beautiful journey.

TABLE OF CONTENTS

LIST OF FIGURES

LIST OF TABLES

ABSTRACT

Additive manufacturing provides a distinctive layer-wise production method, which is efficient and effective, especially when fabricating products with complex designs and/or multiple materials. One of the promising applications of additive manufacturing is 3D printing flexible piezo-resistive sensors, which measure the strain of human motions by characterizing the changes in resistance. In this research, fused deposition modeling is used to fabricate stretchable piezo-resistive sensors that use thermoplastic polyurethane (TPU) as the stretchable layer and the mixture of TPU and carbon nanotube (CNT) as the electrically conductive layer. Extensive experimental efforts are dedicated to investigating proper mixing technique, filament preparation method, and a range of process parameter settings. To evaluate the quality of 3D printed stretchable piezo-resistive sensors, multiple measures are used including filament consistency, print quality, gauge factor, and electromechanical properties from static and dynamic testing. In this study, 7.5 wt.% CNT in the TPU-CNT mixture is chemically prepared (with solvent), its feasibility of being made into 3D printing filament, and 3D printability are investigated.

During the static electromechanical testing, the printed sensors are stretched to 10%, 20%, 30%, and 40% strain. The obtained gauge factor which is computed as the ratio of change of resistance to strain is decent overall (over 2 in most cases) but it is relatively less for lesser strain in some cases. If the gauge factor can be increased for smaller strains as well, the sensor with its high sensitivity will have potential applications in wearable electronics and health monitoring systems. In addition, during 10 cycles of dynamic electromechanical testing for 20%, 30%, and 40% strain changes, the resistance change is found to be the most consistent for 30% strain change.

1. INTRODUCTION

1.1 Additive Manufacturing

The manufacturing industry is continuously changing to reduce cost, reduce energy and resource use, and expand manufacturing capabilities [1,2]. Rapid changes have occurred in the manufacturing sector because of the introduction of innovative manufacturing techniques and the rising demand for personalized products. Over the years, the manufacturing industry has advanced, owing to the rapid growth of additive manufacturing (AM), often known as 3D printing. Due to its uniquely enhanced manufacturing complexity and design freedom, AM is making a significant impact on modern manufacturing practices [3]. The door for AM has opened as the industry plans to place a greater emphasis on individualized client needs than mass output [3]. Stereolithography, a process Charles Hull invented in 1986, was followed by other innovations such as powder bed fusion, fused deposition modeling, inkjet printing, and contour sculpting [4].

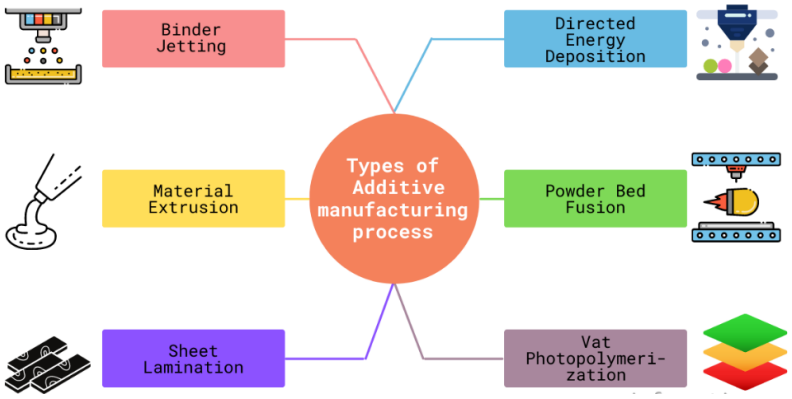

Figure 1. Different types of AM technologies [5]

AM is a process in which a physical object is constructed by printing one layer at a time from computer designed model [6,7]. Traditionally, material is either removed by machining, grinding, or drilling or it is cast into molds in subtractive manufacturing or formative manufacturing, but in AM, a part is produced layer by layer which yields more freedom in design to produce complex

parts [2]. Different AM processes have different forms, such as material extrusion, binder jetting, directed energy deposition, powder bed fusion, sheet lamination, and vat polymerization. In the process of material extrusion, materials are selectively dispensed from the nozzle; in the binder jetting process, a liquid bonding agent is deposited to join powders; in directed energy deposition, materials are melted as they are deposited; thermal energy is used to fuse specific regions of the powder bed in powder bed fusion process; materials are bonded in sheet lamination procedure, and liquid photopolymer in a vat is selectively cured by light-activated polymerization during the process of vat polymerization [8]. The most widely utilized technologies nowadays are stereolithography (SLA), fused deposition modeling (FDM), selective laser sintering (SLS), metal additive manufacturing (MAM), and direct metal laser sintering (DMLS) [9]. FDM works by extruding heated thermoplastic filament; the liquid resin is cured in a laser in SLA; a laser is used to fuse small plastic, metal, or ceramic powder particles in SLS; the powder is fused by an energy source to create metal parts in MAM, and small particles of metal powder are fused by laser in DMLS [5]. The types of AM processes and how AM works are shown in Figure 1 and Figure 2.

AM is advantageous not only in terms of producing parts with complex geometry but also in combining multiple materials within a single print. However, design for additive manufacturing (DFAM) is a still work in progress. The accepted practices have not yet

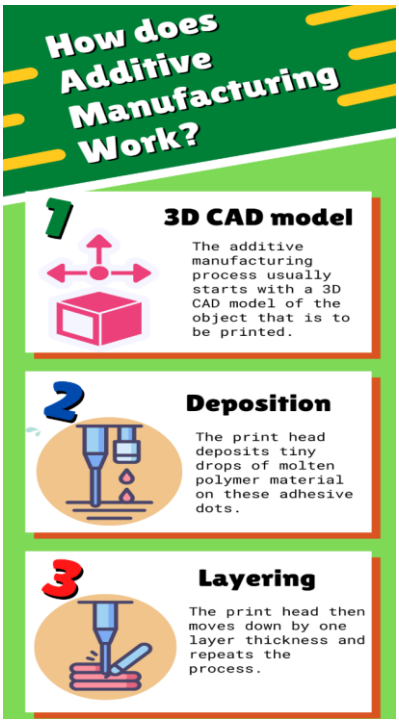

Figure 2. Brief working process of AM [5]

been established. The lack of standardization has prevented Quality Control (QC) from certifying AM for industrial use [2]. Another significant problem with AM is that printed objects can occasionally have flaws, and prints made using the same digital input can have different surface roughness. As a result, poor tolerance and surface quality are traded for geometric complexity in AM [10]. The major advantages and challenges of AM are shown in Table 1.

Table 1. Advantages and Challenges of AM

Advantages of AM	**Challenges of AM**
No tools or molds are needed because the part is printed directly from the CAD model.	Higher production cost.
It offers design freedom while producing highly personalized items.	Decreased production pace.
Materials left over from manufacturing can be used again for future printing.	Standardization has not yet been developed for industrial usage.
Sharing CAD models is simple, which makes it easier to make design changes	Post-processing of manufactured parts is occasionally necessary.
Items with multiple colors and materials and embedded electronics can be created	Sometimes variations in parts generated from the same CAD design are observed.
It reduces lead time and inventory cost by producing products as needed only.	In some cases, the printed part has defects.

Several major industries, including aviation, automotive, healthcare, and consumer goods are now using 3D printing. AM technologies are used to create aircraft engine brackets, landing gear components, wall panels, air ducts, and seat frames [11]. 3D printing of brake parts, air vents, gasoline tanks, custom seats, automotive brackets, and other parts is a common practice in the automobile industry [12]. Some frequent applications of AM in the medical sector include dental implants, anatomical models for surgery, specialized medical tools like forceps, clamps, hemostats, and retractors, and wearable sensors for detecting human motion [13]. Additionally,

3D printing is now used to create consumer goods including eyeglasses, hearing aids, wearable technology, bike fiber, helmets, shoe insoles, etc. [14].

1.2 Additive Manufacturing of Sensors

With the advancement of AM technologies, several types of sensors are produced for a variety of applications. Traditional manufacturing processes for sensors result in higher costs, longer production times, and more importantly, less design adaptability [15]. In the current literature, researchers aim to create 3D-printed sensors with more customizability and lower manufacturing costs [15]. Sensors can be classified into three types: physical sensors, chemical sensors, and biosensors [16]. Changes in physical quantities are detected by physical sensors, which convert the changes into electrical impulses [16]. An example of a physical sensor is a tactile sensor which collects data from physical interactions with its environment. When an external load is applied to a tactile sensor, mechanical impulses are converted into electrical signals and those electrical signals are then detected with the help of an external analyzer [17]. Wearable tactile sensors must possess the following qualities to mimic the functionality of human skin: high flexibility and stretchability so that it can be worn on the skin and attachable to it; high sensitivity to detect strain, pressure, torsion, or shear; repeatability over cyclic loading and unloading; linearity in input-output characteristics; and quick response to cyclic loads [17]. However, the incorporation of such properties is a challenge. Flexible tactile sensors use a variety of sensing techniques, including capacitive, piezoelectric, and piezo-resistive mechanisms [17]. The sensing film in piezo-resistive sensors converts mechanical impulses into resistance or conductance change, which is then measured by an external circuit; piezoelectric sensor, as its name suggests, converts changes in strain, pressure, acceleration and force into quantifiable electrical quantities; and capacitive

sensors function by detecting changes in capacitance in the dielectric layer positioned between electrodes [17].

3D-printed flexible piezo-resistive strain sensors demonstrate resistance change when the sensors go through strain changes, and they have potential applications in wearable electronics, electronic skin, and health monitoring systems [18]. Traditional piezo-resistive strain gauge has the drawbacks of being a fixed directional sensor and measuring only extremely small strains [19]. Sensing components like nanoparticles are used to suit the needs of flexible tactile sensors to be incorporated into wearable electronics. The sensing layer of the sensor has been 3D printed using a variety of nanomaterials, such as graphene [20–22], CNT [23–25], gold [26], silver [27], metal nanoparticles [28], etc.

1.3 Fused Deposition Modeling

FDM is also referred to as fused filament fabrication (FFF), and it belongs to the domain of material extrusion. The materials used are thermoplastic polymers that are available as filaments. When heated, thermoplastic material softens; when cooled, it hardens. Thermoplastics do not change their chemical characteristics after repeated heating and cooling. An FDM printer consists primarily of three components: the build platform, the filament coil, and the extrusion head or extruder. The printer is first fed with a spool of thermoplastic filament. The filament is injected into the extruder once the nozzle reaches the required temperature. The extruder's function is to feed the filament from the reel to the hot end. The hot end contains the nozzle where the filament is melted. The extruder is capable to move in the x, y, and z planes. The extruded material is deposited layer by layer in preset locations, where it cools and solidifies, in thin strands. To speed up cooling, a fan can be fastened to the extruder. Multiple passes are needed to fill a space. The build platform moves down or the extruder moves up and deposits a new layer after each completed

layer. Until the part is finished, the procedure is repeated. Nozzle temperature, bed or platform temperature, print speed, primary layer height, print infill density, and nozzle diameter are among the most important process parameters. These settings need to be chosen accordingly based on the type of print required and the type of filament used. A layer with a lower height creates sections that are smooth and can capture curved geometry. Greater height produces parts cost-effectively and in less time. The higher the infill density, the stronger the printed object. Higher print speed will produce the part quicker but quality can be decreased. The build platform size and the cooling fan speed are also important. The most popular FDM materials are ABS (Acrylonitrile Butadiene Styrene), PLA (Polylactic Acid), and TPU (Thermoplastic Polyurethane). Although ABS is strong and resistant to temperature changes, it can warp. PLA is simple to print and has an aesthetic quality, but it has poor impact strength. TPU is incredibly flexible, however, printing with accuracy can be challenging. The working process of FDM is illustrated in Figure 3.

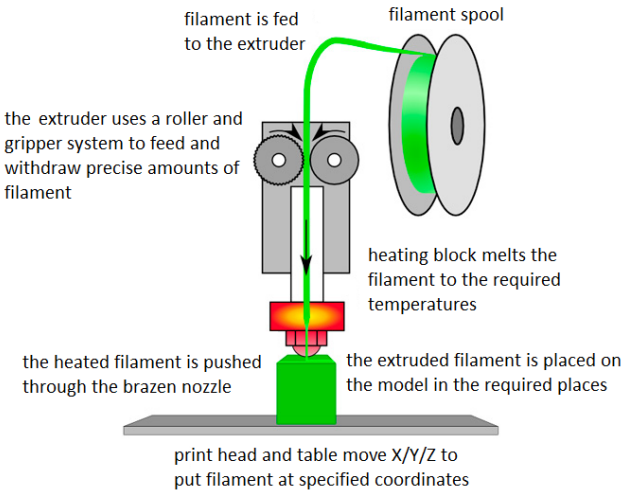

Figure 3. The FDM process [29]

2. LITERATURE REVIEW

In this section, related work regarding the printing of strain sensors is discussed. Most of the papers have used FDM printer [6,18,21,24,25,27,30,31]. FDM is one of the most common 3D printers because of its low cost. Some papers have employed the dual-nozzle FDM printer to independently extrude two different materials without needing to pause the printing process [21,25]. As far as the process parameters for printing are concerned, nozzle temperature of 220℃ [24,25] or 230℃ [21,30], bed temperature of 60℃ [21,24,25], printing speed of 20 mm/s [24,25,30], primary layer height of 0.2 mm [18,21,24,25,27,30], print infill of 100% [21,24,25] and nozzle diameter of 0.4 mm [6,21] and 0.8 mm [24,25] have been widely used. Although printing is trickier with TPU, its unparallel flexibility makes it very useful for printing stretchable sensors. Hence most of the papers have used TPU for printing the base layer or the substrate [21,24,25,27,30,31]. For printing the sensing film, conductive materials such as CNT [18,24,30,32], graphene [20,21], and silver [27,33] have been used mostly. The thickness of the printed sensor usually varies between 1 mm and 2 mm [18,21,24,31]. Two types of structure are mostly common: printing the sensing layer in a zigzag pattern on the substrate [6,9,33,34] and printing the sensing layer with the substrate layer on top and bottom of it (sandwich structure) [20,25].

Over the years, the printing of piezo-resistive strain sensors has gained the attention of many researchers and as a result, different materials and fabrication techniques have been used. Special interest has been shown in conductive polymer composites (CPCs) that contain carbon-based fillers. A multiwalled carbon nanotube (MWCNT) was used by Christ et al. [25] as the filler for its excellent conductive properties when composited within the thermoplastic. TPU filament containing 3 wt.% MWCNT was produced. A dual-nozzle FDM printer was used. First, while the

second nozzle was parked, the first nozzle extruded TPU to construct the substrate. Second, while the first nozzle was parked, the second nozzle extruded TPU/MWCNT to print the conductive layer. Finally, while the second nozzle was stalled, the first nozzle extruded TPU. The conductive pattern of MWCNT/TPU was sandwiched between the flexible substrate of TPU. Christ et al. [24] printed the base part using only TPU and the sensing part using 2 wt.% CNT/TPU, 3 wt.% CNT/TPU, 4 wt.% CNT/TPU, and 5 wt.% CNT/TPU. The obtained gauge factor (GF), which is a measure of sensitivity was 18.2, 9.2, and 8.6 for 3 wt.% CNT, 4 wt.% CNT, and 5 wt.% CNT respectively. Vu et al. [30] printed a strain sensor using a commercial conductive flexible filament made of CNT/TPU. The effects of printing line directions at 45°, 90°, and 180° were studied. Results indicated that printing in a 45° direction is the best way to improve the sensor's properties. GF was found to be 21.5, 16.2, and 10 for (0-2)%, (2-4)%, and (4-8)% strain respectively. However, the sensor could only be stretched up to 8% strain. Yu et al. [18] used CNT/thermoplastic elastomer for making the conductive part of the sensor and concluded that the GF decreases as the thickness of the conductive layer increases. The GF value also decreases with the increase of the CNTs' suspension concentration. CNTs' suspension concentration of 0.0025 g/mL had the highest GF value of 6.85.

In addition, Munasinghe et al. [6] printed the conductive layer of the sensor using commercial conductive filament which was a mixture of PLA and carbon black, and printed the base layer using PLA filament. Kouchakzadeh et al. [9] used TPU and ABS/carbon black to print the substrate and the conductive channel respectively. Two sensors were printed, one with two conductive channels and the other with four conductive channels. It was concluded GF is more for the sensor with more conductive channels. It was also found that GF increases as the thickness of the conductive channel decreases.

Alsharari et al. [21] printed the conductive layer by co-printing conductive Graphene based Polylactic Acid (GP) with TPU and printed the base layer or substrate with only TPU in an FDM printer. Three 3D printed samples with mass loadings of GP, GP-10TPU (mass loading 10% of the TPU added to GP), and GP-20TPU were prepared. The printed sample showed the highest sensitivity when GP-10TPU was used. It was concluded that the co-printing of Graphene/PLA/TPU in a meander sine-wave structure increased the stretchability. Mousavi et al. [31] used TPU for printing the structural layer and PLA-Graphene for printing the conductive layer, and the goal of the sensor was to measure the bending angle of soft actuators. PLA-G was sandwiched between TPU as the top and the bottom part of the sensor contained TPU and the middle part was PLA-G. This unique design of the sandwich structure helped to increase stretchability.

The Wyss Institute at Harvard University created a novel hybrid 3D printing method (2017) [35]. The process involved picking and placing electronic components after printing elastic conductive inks to create flexible and wearable sensors. The device's underlying soft substrate and conductive electrodes were made from pure TPU and silver-TPU inks, respectively. There is complete control over the pattern of conductive features because both the ink and substrate are 3D printed, and it is feasible to construct circuits to create soft electronic devices of almost any size and shape. Submicron-sized silver particles were combined with a highly stretchy silicone elastomer to create a new ink by Li et al. [36]. Tactile sensors were fabricated in as many as six layers: base layer – silicone, bottom electrode – 75 wt.% Ag/Si, sensor layer – 68 wt.% Ag/Si, isolating layer - silicone, supporting layer – 40% Pluronic, top electrode – 75 wt.% Ag/Si. The inks were employed to create printed flexible, elastic, and sensitive sensors that can recognize and distinguish between human movements such as the radial pulse, finger pushing, and bending. Li et

al. [27] used Ag/TPU to print wearable sensor and carried out microwave heating as a part of post-processing. It was found that microwave heating heats Ag selectively and the irradiated Ag heats TPU. As a result, the microstructure is improved because the gaps in the composite are reduced. This MW heating also increased the tensile strength and the elongation at break.

Apart from the FDM process, other new printing technologies have also been implemented to print strain sensors. Muth et. al [34] used embedded 3D printing (e-3DP). Carbon conductive grease as ink was employed for sensing material and silicon elastomer as reservoir and filler fluid. The obtained GF was between 3.2 and 4.4. Moorthi et al. [33] used screen printing to print strain sensor. Liu et al. [17] evaluated the most recent developments in printing technology and printable materials. Direct Ink Writing (DIW) and FDM are materials extrusion-based 3D printing processes. FDM is straightforward and reasonably priced. Typically, in FDM, the substrate and dielectric layer for tactile sensors are made using TPU. Piezo-resistive sensing elements are made using FDM from composite materials made of thermoplastic polymer and conductive polymers, such as polycaprolactone/carbon black and TPU/MWCNT. Many kinds of printable composite ink can be produced with DIW by dispersing conductive fillers like carbon black, MWCNT, graphene, metal nanoparticles, or nanowires into elastomeric materials like silicone elastomer. Stretchable substrate, electrodes, and sensing elements can be created using these printable inks. The benefits of DIW include its wide range of printable materials and its capacity to extrude silicone elastomer with the greatest stretchability. A more competitive 3D printing process is DIW, for creating tactile sensors. Meanwhile, Lanzotti et al. [32] examined on the impact of process parameters on the mechanical properties of items manufactured in PLA. The combination of parameters that maximized the ultimate tensile strength and the elastic modulus by means of the response surfaces, is layer thickness 0.2 mm and infill orientation 0 degree.

Although many studies have been conducted to study carbon-based piezo-resistive strain sensors, the 3D printing of these sensors is not easy to replicate. While making the conductive-flexible filament, the incorporation of one property (conductivity or flexibility) affects the other. The conversion of carbon-based pellets into filament and the printer hardware settings can still be ambiguous. The complexities associated with material mixing, filament preparation, and printer settings are deeply addressed in this report. Instead of using commercial filaments, filaments are prepared in this study. In this research, 7.5 wt.% CNT/TPU is used to print the conductive part of the sensor. To the best of our knowledge, such a ratio of the amount of CNT in TPU has not been used before to print such sensors. The TPU filament is relatively simple to fabricate. But the conductive filament is not easy to make and printing with it is not easy either. This is owing to the addition of CNT into TPU. Due to the physical nature of CNT, certain settings in the extruder and the printer need to be chosen while filament preparation and printing respectively. In this study, at first, the flexible filament is prepared from TPU pellets. Next CNT powder is mixed with TPU powder, pellets are produced from the mixture, and the conductive flexible filament is produced from those pellets. An FDM printer is used to print the base of the sensor with the filament made from TPU and the sensing part is printed from the conductive mixed filament. The sensor is printed according to the predesigned model. The design of the sample is different from regular designs. This design of conductive pattern allows less material consumption. Multiple samples of sensors have been printed to analyze the results and variations. The samples are strained while their resistance is measured to calculate the GF. This test is conducted not only statically but also dynamically.

3. METHODOLOGY

3.1 Principle of Strain Gauge

Strain is the amount of deformation or displacement experienced by a substance. Strain ($\in$) is defined as the ratio of change in length (ΔL) to the original unstressed length of the object (L), as formulated in Equation (1).

$$\in = \frac{\Delta L}{L} \tag{1}$$

If the line element is stretched to twice and three times its original length, then the strain is said to be 100% and 200% respectively, and so on. A strain sensor or strain gauge is an electrical sensor that is used to measure strain. In a resistance-based strain sensor, the resistance varies proportionally to the strain applied on the sensor [6]. Strain gauges are commonly made up of grids of conductive metallic foil or wire. 3D-printed conductive traces can also be used as a substitution for metallic foil or wire and the sensing material can be printed onto the base material, which transfers the strain to the sensing material [6].

Due to the applied load as the substrate experiences strain (elongation), so does the conductive sensing material. When the sensor is stretched, it gets longer and narrower (length increases, cross-sectional area decreases) and therefore its resistance is increased in the two terminals of the sensing material.

The ratio of fractional change of resistance ($\frac{\Delta R}{R}$) is proportional to the strain applied where R is the original resistance in unstrained condition and ΔR is the change of resistance due to straining. The Gauge Factor, GF defines the sensitivity of the strain sensor which is given by Equation (2). GF is defined as the ratio of the fractional change in electrical resistance to the fractional change in length (strain).

$$GF = \frac{\frac{\Delta R}{R}}{\frac{\Delta L}{L}} \quad (2)$$

3.2 CAD Design of the Stain Sensor

The sensor is designed in SOLIDWORKS, as shown in Figure 4. The base part has a length of 10 mm, a width of 100 mm, and a thickness of 1 mm. The conductive layer on the base part has a width of 0.6 mm and a thickness of 0.6 mm. The total thickness of the sensor is 1.6 mm. The lower the thickness of the conductive part, the higher the sensitivity of the sensor. Also, there should be at least two layers to make sure there is no void in the print. A conductive layer thickness of 0.6 mm allows 3 printed layers (each being 0.2 mm) and it is not a large thickness either.

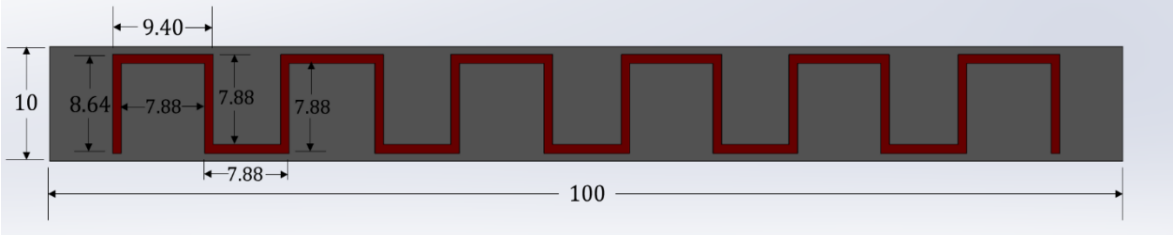

Figure 4. CAD design of the piezo-resistive sensor (unit: mm)

3.3 Materials of the Base part and the Conductive part

The printed sensor has two parts: the base part and the conductive part. The base part is made from the palletized form of TPU. The conductive part is made from a mixture of single-walled carbon nanotube (SWCNT) and the powdered form of TPU. TPU and SWCNT are used as the constituents of the nanocomposite in this study. TPU in pellets form of grade IROGRAN® A 80 P 4699L is purchased from LNS Technologies with Shore Hardness 80A and specific gravity of 1.09 g/cc [37]. TPU in powdered form is purchased from STS Inks, USA having a particle size of 70-80 micrometers [38]. SWCNT in powdered form having purity ≥ 80%, average diameter 1.2 – 2.0 nm, density 1.7 – 1.9 g/cc. is purchased from Sigma-Aldrich [39].

Since the sensor must be stretchable, TPU is perfect in this regard. TPU is known for its high flexibility and toughness. CNT is widely used to develop polymer composites for its excellent electrical and mechanical properties [40]. CNT is a tube-shaped allotropic form of carbon. A carbon atom contains 4 electrons in its outermost orbit. In CNT, each carbon atom is bonded to three other carbon atoms by a strong covalent bond. It means each carbon atom also has a free electron. Hence, a sea of delocalized free electrons is formed within the tube. Therefore, CNT conducts electricity. For polymer composite such as CNT-mixed TPU to conduct electricity, electrons must be able to jump from one CNT to another through a thin polymer layer [40]. Despite the advantage of CNT, it is a very challenging task to uniformly integrate CNT in a polymeric matrix [41]. Moreover, it is difficult to 3D print with a CNT-mixed filament.

3.4 Preparation of the TPU Filament

TPU pellets are extruded in EX6 (Filabot, USA), a single screw extruder with a screw length to diameter ratio of 24:1. With an extrusion temperature of 160℃ and screw speed of 30 rpm, a strand of TPU filament is obtained having a diameter of 1.6 mm. It is important to determine the accurate extrusion temperature and the screw speed for making filament with a uniform diameter. After several experiments, the following optimal parameters shown in Table 2 are found to extrude the filament.

Table 2. Adopted parameters in EX6 for TPU filament fabrication

Front temperature – metering section heat zone (nozzle end)	160 ℃
Middle temperature – compression section heat zone	160 ℃
Back temperature – feed/compression section heat zone	160 ℃
Feed temperature – feed port temperature heat zone	35 ℃
Screw speed	30 rpm

3.5 Preparation of the CNT/TPU Filament

3.5.1 Preparation of CNT/TPU Mixed Pellets

At first, a v-mixer is utilized to mix the pelletized TPU and the powdered CNT to make a dry mixture of 7.5 wt.% CNT/TPU. The mixing speed is 33 rpm, and the duration of mixing is 10 hours. The TPU pellets which are white turned black. It is thought that the CNT powder is mixed with the TPU pellets. In the same single screw extruder, EX6, the dry material is then blended. The mixture filament is created with the same extrusion temperature and screw speed of 160°C and 30 rpm, respectively. Next, the conductivity of the filament is measured. However, the reading shows no conductivity at all. This means that the CNT powder is not properly mixed with the TPU pellets and only the outer surface of the TPU pellets is covered with CNT powder.

Since the use of a v-mixer is a failure, more attention is then given to the proper mixing of CNT into the TPU matrix. For easier and better mixing, TPU in powdered form is purchased because the CNT is in powdered form as well. 92.5-gram powdered TPU is melted in a beaker at 240°C in an oven. After 30 minutes, 7.5-gram CNT is added to the TPU. Then a high-speed mechanical mixer is used to blend the mixture. However, it is very difficult to mix even with the high-speed mixer. It is due to the highly viscous nature of fluidic TPU and agglomerating nature of CNT. The blades of the mixer could hardly rotate. This second process of mixture preparation also has not worked. Mixing could have been easier if it is possible to melt CNT. In CNT, as a carbon atom bonds with another carbon atom, there is a long chain of a stable structure. It takes massive energy to melt it resulting in its very high melting point.

CNT is insoluble in common solvents. The mixture of CNT and an organic solvent with or without polymer is a dispersion of CNT in the medium, not a solution [42]. Isopropyl alcohol (Propanol-2) solution is found to be the best solution to disperse SWCNT using the ultrasonication

process [43]. CNT aggregates very easily and ultrasonication can help to attain discrete nanotubes. Another 7.5 grams of CNT is placed in a beaker containing isopropyl alcohol, and it is ultrasonicated for an hour using DK Sonic, an ultrasonic cleaner. While ultrasonication, it is made sure to stir the mixture. Next, 92.5 grams of TPU powder is added to the mixture. The mixture is again ultrasonicated and stirred for another hour. The isopropyl alcohol is evaporated by heating the mixture in the oven at 90°C. The mixture of TPU and CNT is dried at room temperature for 24 hours. This mixture of solid mass is cut into smaller pieces. Next, those pieces are fed into a pelletizer to make pellets.

3.5.2 Preparation of CNT/TPU Filament

The 7.5 wt.% CNT/TPU pellets are extruded in the same extruder, EX6. Before feeding the CNT-mixed TPU pellets into the extruder, it is made sure that the residual TPU pellets are removed. After removing the nozzle from the machine some purging materials are extruded as directed by the operation guideline of the machine. The screw is removed from the machine to clean the barrel. The screw and the nozzle are cleaned. After loading the screw and nozzle, the extrusion temperature is set to 135°C which is found to be the right temperature after many experiments. The CNT-mixed TPU filament is obtained having an average diameter of 1.75 mm. It is made sure that the filament is extruding straight and tightly to keep the diameter of the filament constant and avoid its twisting. If a much higher proportion of CNT is used to increase conductivity, then there is a possibility that the filament will be more brittle causing it to break very easily when stretched or bent. It will be very difficult to 3D print using such kind of filament. The parameters used to fabricate the conductive filament are listed in Table 3. TPU pellets, TPU filament, CNT powder, TPU powder, mixture of CNT and TPU powder, mixed pellets, and mixed filament are shown in Figure 5.

Table 3. Adopted parameters in EX6 for CNT/TPU filament fabrication

Front zone temperature	135 ℃
Middle zone temperature	135 ℃
Back zone temperature	135 ℃
Feed temperature	40 ℃
Speed	30 rpm

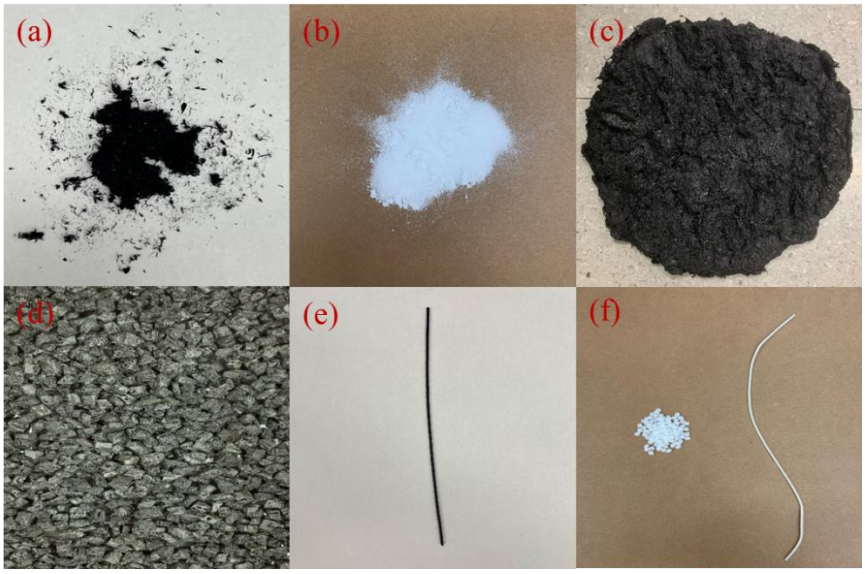

Figure 5. Illustrations of (a) CNT powder, (b) TPU powder, (c) CNT-TPU mixture, (d) CNT-TPU mixture pellets, (e) CNT-TPU filament (f) TPU pellets and TPU filament

3.6 Fabrication of Stretchable Sensors

During mechanical testing, the sensor is stretched along the width. Simplify3D, a 3D printing slicing software, is used to convert 3D models into printable formats and to operate the printer and printing process. The sensor is printed using an FDM printer manufactured by Creality 3D, China, model Ender 3. At first, the TPU filament is loaded into the printer and the base part is printed. Next, the TPU filament is unloaded and the CNT-mixed TPU filament is loaded. Finally, the conductive part in a zigzag pattern is printed on the base part. Printing the base part is routine but printing the conductive part is not easy. After many failed printing attempts, some critical

considerations are identified to be able to print using a filament that contains CNT and they are as follows:

i. The filament is dried for four hours at 50℃ using a dryer. Before printing, the filament needs to be free from moisture.

ii. A nozzle made of brass may not work to print filament containing CNT. CNT is abrasive. Hence nozzle made of steel is used to print in this experiment.

iii. A nozzle having a large diameter (0.8 mm) is used to avoid nozzle clogging while printing [44].

iv. The filament loading and the unloading path should be as small as possible. Instead of a Bowden extruder, a direct-drive single-gear extruder is used. The filament path between the extruder and the hot end is much shorter in a direct drive than in a Bowden extruder.

The process parameters used in the slicing software for printing are listed below in Table 4. The printed sensor is shown in Figure 6.

Table 4. Adopted parameters in 3D printing

Process Parameters	**Base layer**	**Conductive layer**
Nozzle diameter	0.8 mm	0.8 mm
Nozzle temperature	220 ℃	230 ℃
Bed temperature	60 ℃	60 ℃
Layer thickness	0.2 mm	0.2 mm
Print speed	400 mm/min	400 mm/min
Infill density	100 %	100 %

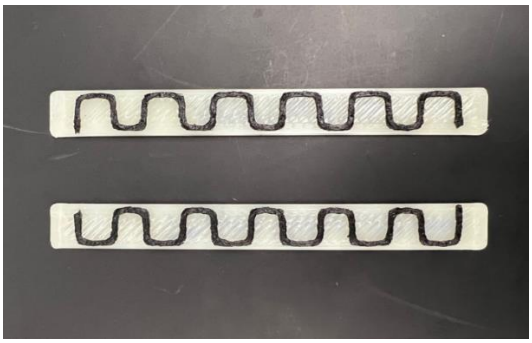

Figure 6. The 3D printed piezo-resistive strain sensor

3.7 Experimental Design

A digital microscope, Keyence VHX-7000 is used to capture the images of the conductive layers. The differences in the width of the conductive layers due to printing variability among the printed sensors are captured and measured with this microscope. In addition, Hitachi S-3000N Scanning Electron Microscope (SEM) is used to focus on the conductive layer. A universal testing machine (UTM) is used to investigate the sensor's tensile performance, as well as their piezo-resistive performance. Stretching causes the sensor's conductive sensing material to deform. As a result, its resistance changes. A digital multimeter (Model: 2831E, B&K Precision Corp.) is used to measure the change in resistance by connecting its two lobes to the endpoints of the conductive part of the sensor. A computer is connected to the multimeter. The data is saved to the computer. For static testing, each of the four replications of strain sensors is stretched to 10%, 20%, 30%, and 40% strain, and their corresponding values of resistance are noted and therefore, GF is calculated. Apart from measuring the GF, each of the four samples is continued to stretch even after 40% strain till failure to determine the failure strain. Hence the first four printed samples are used not only to perform static electro-mechanical testing to determine GF but also to determine the failure strain. For cyclic testing, another six replications of sensors are printed. Two samples are loaded to 20% strain and unloaded to 0% strain and the cycle is repeated 10 times. In the same

way, cyclic testing was done for another two samples with 30% strain and two more samples with 40% strain. The corresponding values of resistance are noted from the multimeter reading. The setup of tensile testing and simultaneous measurement of resistance is shown in Figure 7.

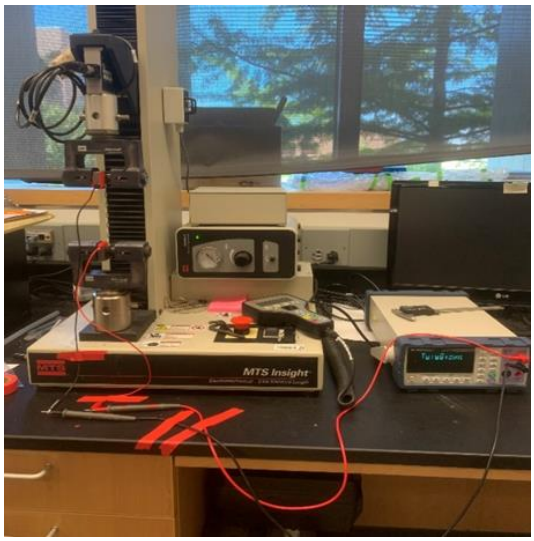

Figure 7. The experiment equipment (including the UTM and the multimeter)

4. RESEARCH RESULTS

4.1 Microstructure

Microscopic images are captured to determine the width of the middle region of every conductive line (which are parallel to the length) of sample #1, #2, #3, and #4. The measured width of the samples is shown in Table 5. It is seen that there are variations in the width of the samples and the average and standard deviation are shown in Figure 9. A sample image to measure the width of the middle region of a conductive line of a sample and a sample SEM image of a conductive line are shown in Figure 8.

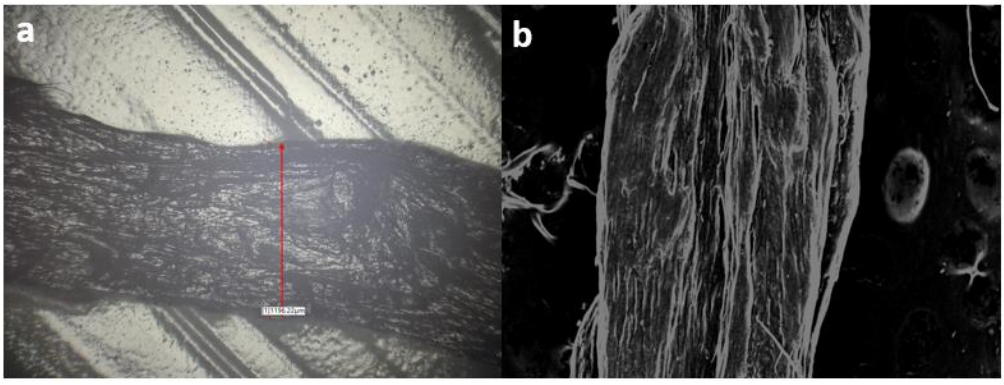

Figure 8. (a) Microscopic image to measure width of conductive line, (b) SEM image of conductive line

Table 5. Width of the middle region of the conductive lines in millimeters (along the length of the sample)

	Sample #1	**Sample #2**	**Sample #3**	**Sample #4**
Line 1	0.58629	0.60406	0.69754	0.66915
Line 2	0.61941	0.52357	0.60053	0.74724
Line 3	0.62831	0.54783	0.61768	0.66739
Line 4	0.63124	0.66973	0.62532	0.79927
Line 5	0.61290	0.53897	0.64544	0.62370

Line 6	0.56917	0.57931	0.67088	0.66141
Line 7	0.63598	0.55552	0.68212	0.63014
Line 8	0.55434	0.62769	0.62534	0.54432
Line 9	0.63006	0.63473	0.70757	0.65610
Line 10	0.65727	0.67326	0.59811	0.68808
Line 11	0.56799	0.60822	0.54369	0.60588
Line 12	0.58806	0.73598	0.63184	0.68449
Average	0.60675	0.60824	0.63717	0.66476
Standard Deviation	0.03253	0.06372	0.04683	0.06523

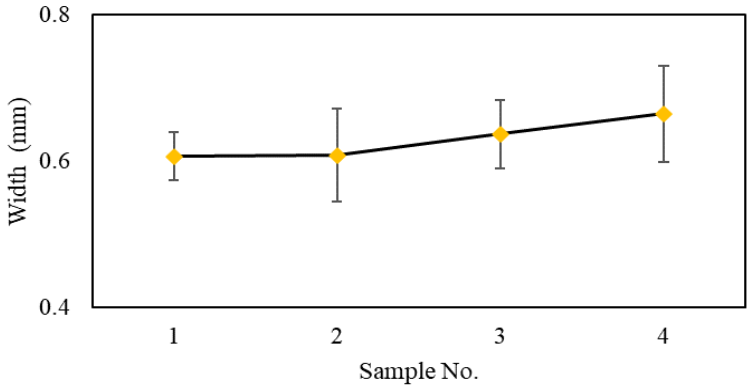

Figure 9. The mean and the standard deviations of width of the middle region of the conductive lines (along the length of the sample)

4.2 Mechanical Properties

To test the stretchability of the sensor, four samples are printed. Using the UTM, tensile testing is performed on all four samples. The failure strain for sample #1, sample #2, sample #3, and sample #4 is found to be 60%, 129%, 111%, and 101% respectively. By failure, the failure of the conductive part of the sensor is meant. It is rational that the base part would break at a much higher strain. This is because the base part is solely made of flexible TPU while the conductive part is made of TPU and CNT. Apart from sample #1, all other samples showed very high stretchability.

These high values of failure strain indicate good layer-by-layer bonding between the base part and the conductive part during printing. In terms of stretchability, sample #1 can be considered an outlier and its early failure might be caused due to some defect in printing leading to a weak bond between the base part and the conductive part. The failure strain is shown in Figure 10. Small black rectangles indicate the strain at which the conductive part of the sample breaks. Figure 11 shows how the conductive layer breaks during the experiment.

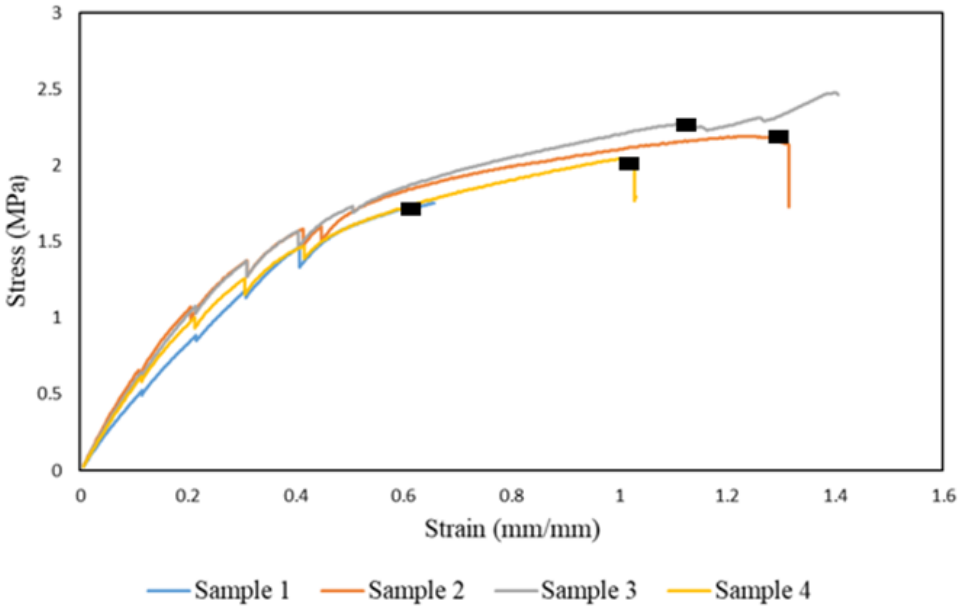

Figure 10. The stress-strain curve of the samples showing the failure strain

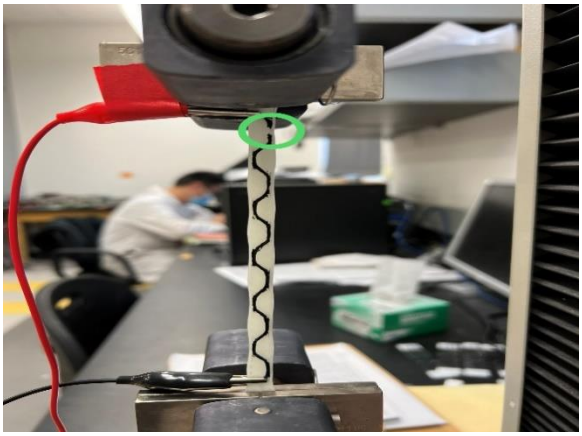

Figure 11. Breaking of the conductive layer during tensile testing

4.3 Electro-mechanical Properties: Static Test

At first, resistance is measured for all four samples. The resistance is measured across the two ends of the conductive part of each sample using the digital multimeter. This is the starting resistance at 0% strain. Sample #1, sample #2, sample #3, and sample #4 have a starting resistance of 18.7 K Ohm, 14.8 K Ohm, 8.6 K Ohm, and 8.7 K Ohm respectively. Each of the four samples is stretched to 10%, 20%, 30%, and 40% strain using the UTM, and the corresponding values of resistance at 10%, 20%, 30%, and 40% strain are measured using the multimeter.

As the sensor experiences tensile load, there is an increase in its length which in turn increases the resistance across the ends of the conductive part. From the point of view of microstructure, cracks tend to develop at the stress-concentrated areas on the sensing film while stretching. The fast separation of nanoparticles at the microcrack edges restricts the electrical conduction paths which cause the electrical resistance to increase upon stretching [45]. The ratio of the increase of resistance to the increase of length which is termed as GF of the sensor is calculated. The higher the density of crack arrays, the more the GF [46]. Since GF is a measure of the sensitivity of the sensor, a higher GF is desired. GF of the four samples at different strains are listed in Table 6. The ratio of change of resistance to different strain values for the four samples is shown in Figure 12.

Table 6. Gauge factors of sample #1-#4

Strain	**Sample #1**	**Sample #2**	**Sample #3**	**Sample #4**
10%	0.68	2.38	0.87	2.98
20%	1.47	3.56	1.81	3.07
30%	3.40	4.21	3.24	7.54
40%	3.57	4.20	5.94	7.78

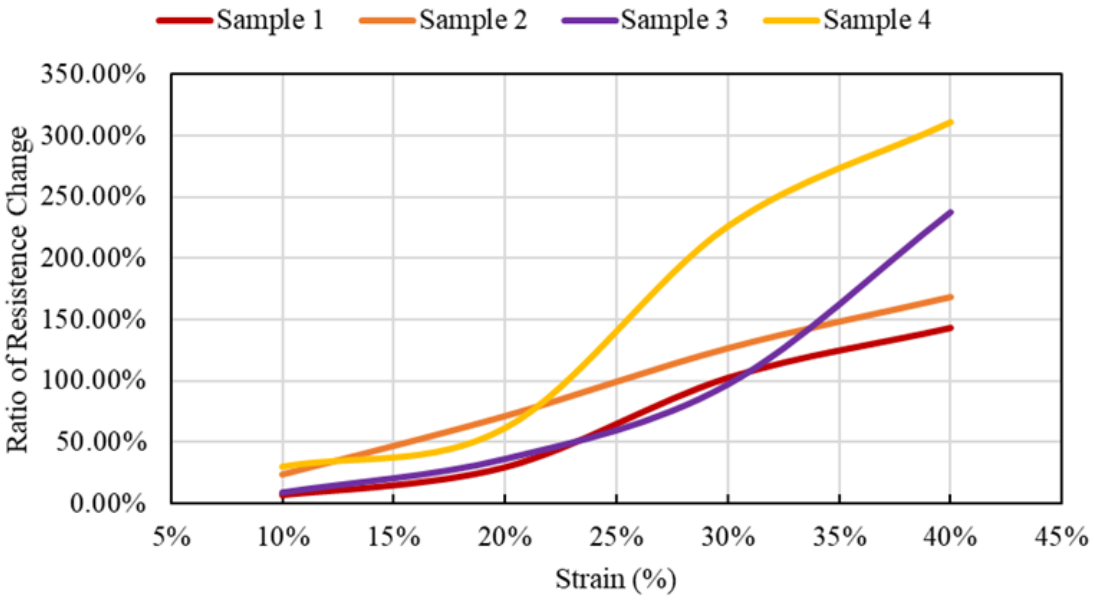

Figure 12. The static testing results

Metal strain gauges typically have a GF of 2. Figure 12 shows that sample #2 exhibits a decent GF and desirable linearity is observed at strain values. Sample #4 also shows good GF values. However, GF increases almost exponentially in sample #4 after 20% strain breaking the linearity pattern. This nonlinearity in piezo-resistive strain sensors is caused due to non-homogenous and microstructural and morphological changes in the conductive films while being stretched [45]. Piezo-resistive strain sensor typically shows a more nonlinear electro-mechanical response than an optical or a capacitive sensor and more specifically, CNT-based polymer composite generally shows nonlinear electromechanical behavior [45]. In terms of electro-mechanical response, sample #2 shows the best linearity, sample #1 also shows decent linearity, sample #4 shows linearity in three regions while sample #4 exhibits some linearity at the beginning and the end but a curvature at the middle. Both samples #1 and #2 show GF of less than 1 at 10% strain while less than 2 at 20% strain. However, these two samples display satisfactory GF once they are strained more than

20%. At low strain, dense cracks may not have formed in the sensing films of these two samples resulting in low GF.

Although the samples should have potential applications in wearable sensors, the GF is on the lower side compared to most CNT-based strain sensors. The GF is 18.2, 9.2, and 8.6 while using 3 wt.% CNT, 4 wt.% CNT, and 5 wt.% CNT respectively [24]**.** This indicates that there is a decreasing pattern of GF with the increase of CNT content. 7.5 wt.% CNT is used in this study and as per expectation, lower GF is obtained which is consistent with [24]. At low CNT content, it is assumed that interconnections of CNT become more sensitive to deformation which is not possible at high CNT content [24]. A higher concentration of CNT suspensions increases its density in the TPU matrix. The more the amount of CNT in the conductive path, the less the influence of the decrease of CNT in the conductive path on the resistance of the sample, and therefore, GF decreases with the increase of CNTs' concentration [18].

There is variation among the resistance of four printed samples in unstrained condition. It is seen that the conductive part of the sensor is not printed very consistently. The width of the printed zigzag-pattern line seems to be varying. This is the disadvantage to print using a nozzle that has a large diameter. To prevent clogging in the nozzle owing to the presence of aggregated CNT, a nozzle with a large diameter has been used for printing and such a large nozzle compromises the consistency of printing. On the contrary, a nozzle having a small diameter ensures fine printing but is unlikely to work when the target is to print a CNT-mixed filament. Hence, nozzle size accounts for this undesirable variation in printed conductive lines. The variation of width is evident among samples from Figure 9 and Table 5. Sample #1 has a lower average width than sample #4. It is known that the resistance of the conductor will be low if the area of the cross-section of the conductor is high due to their inverse relationship. If the width of the conductive part is more, more

electrons can flow increasing conductivity. Therefore, the fact that sample #4 has a higher average width than sample #1 agrees with the explanation behind sample #4's lower starting resistance than that of sample #1.

It has been observed that there are differences among the GF of the samples. It is believed that the difference in the distribution of CNT in the TPU matrix is the reason behind this variation. A study with the help of a more powerful and high-resolution scanning electron microscope should be able to capture the CNT's distribution in the TPU matrix of the samples. Although the target was to prepare 7.5 wt.% CNT/TPU mixture for the filament, it is most likely that the distribution is not uniform throughout. Theoretically, it can be said that the sample showing higher GF is likely to contain less than 7.5% CNT while the sample with lower GF should contain more than 7.5% CNT. A relatively homogeneous distribution of CNT is indicated by the presence of several individual nanotubes [25]. A higher CNT concentration represents a higher aggregate ratio, which means a poor dispersion of nanomaterials in the matrix [47].

4.4 Electro-mechanical Properties: Dynamic Test

Under the tensile load using the UTM, samples #5 and #6 are stretched to 20% strain and unloaded back to 0% strain, sample #7 is allowed to stretch to 30% strain and unloaded back to 0% strain, and sample #9 and #10 are stretched to 40% strain and similarly unloaded back to 0% strain. In this way, 10 cycles are repeated for all these samples. As the samples are stretched, each of their corresponding resistance is determined by the multimeter. Sample #8 is not used as a test specimen because it is a failed print. The corresponding resistance at strain values for samples #5-#6, sample #7, and samples #9-#10 are shown in Figure 13, Figure 15, and Figure 17 respectively. The ratio of change of resistance for 10 cycles for samples #5-#6, sample #7, and samples #9-#10 are shown in Figure 14, Figure 16, and Figure 18 respectively in the form of a histogram.

For samples #5-#6, there is a slight upward trend of resistance as the number of cycles increases as shown in Figure 13. Considerable difference in the output resistance is observed between samples #5 and #6. Figure 14 shows that during the cyclic test at 20% strain, for either sample, the ratio of resistance change never reaches 50% and this low resistance change should be improved.

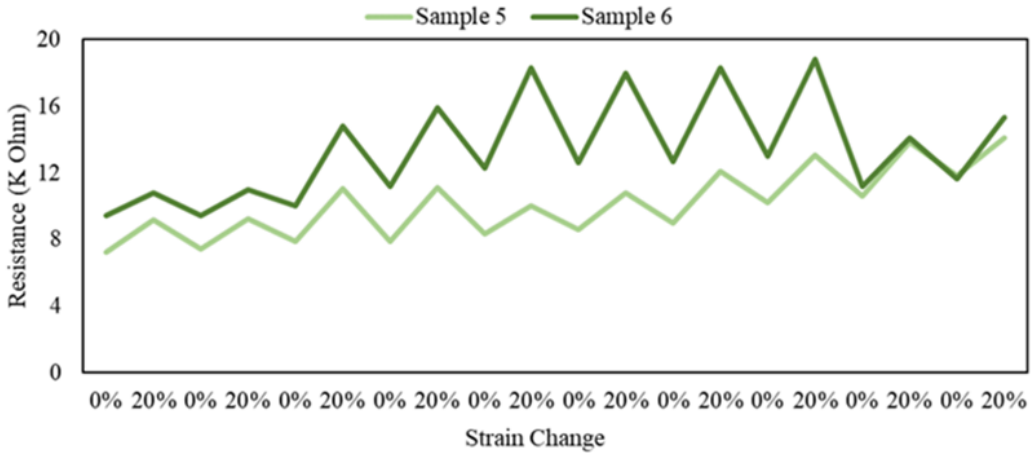

Figure 13. The resistance changes under the 20% cyclic strain change

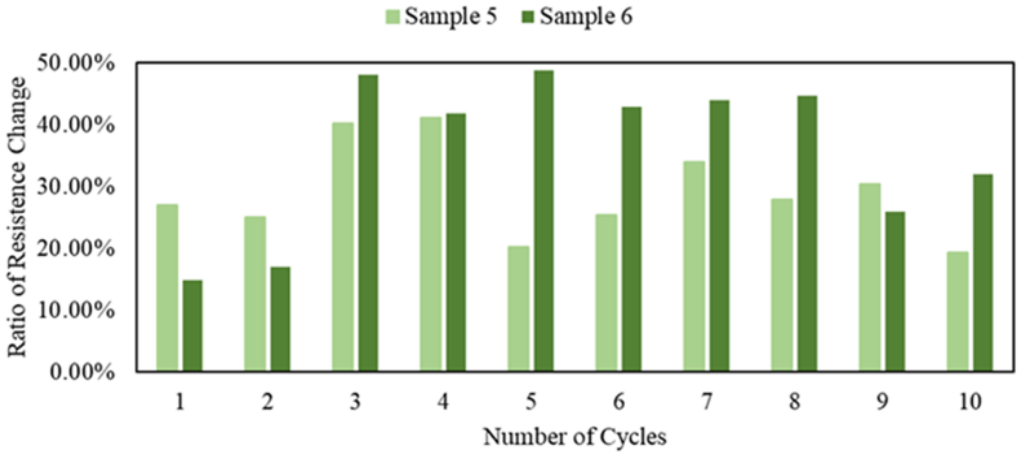

Figure 14. The $\Delta R/R$ changes under the 20% cyclic strain change

Sample #7 which is dynamically stretched for 30% strain shows the best result as shown in Figure 15. The resistance change is very high, around 400%, and very consistent among all the cycles as shown in Figure 16.

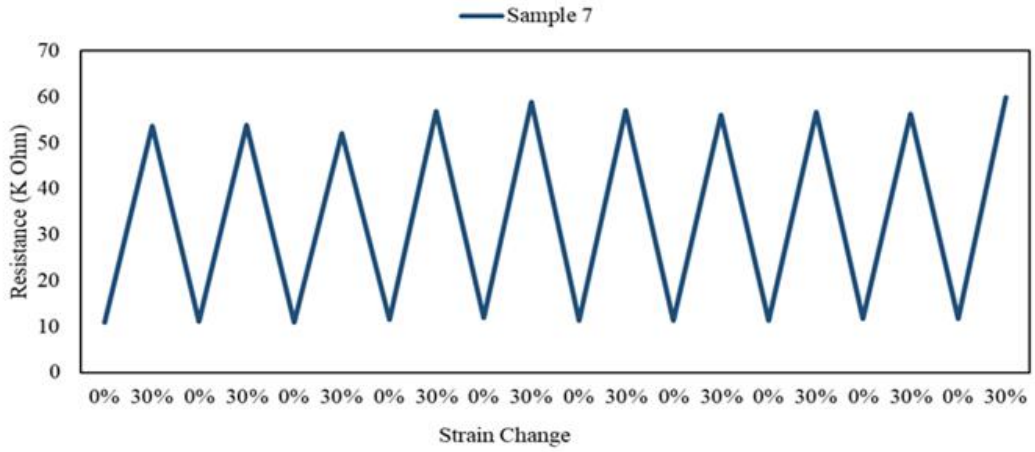

Figure 15. The resistance changes under the 30% cyclic strain change

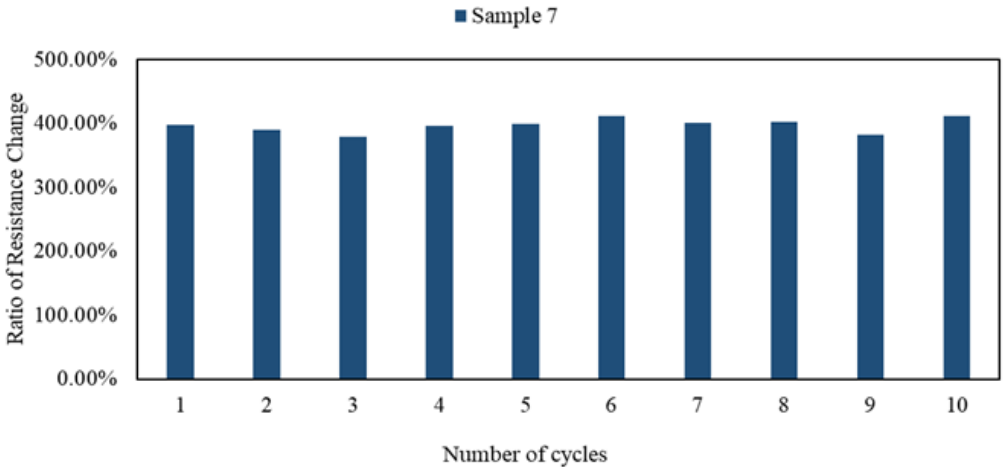

Figure 16. The $\Delta R/R$ changes under the 30% cyclic strain change

For cyclic testing at 40% strain, the ratio of resistance change is quite consistent except for the 9th and 10th cycle of sample #9 where the change crosses more than 150% as shown in Figure 18. In theory, resistance should increase with straining. Comparing Figure 17 with Figure 15, it is seen

that output resistance is less for 40% cyclic straining than that for 30% cyclic straining which must be investigated.

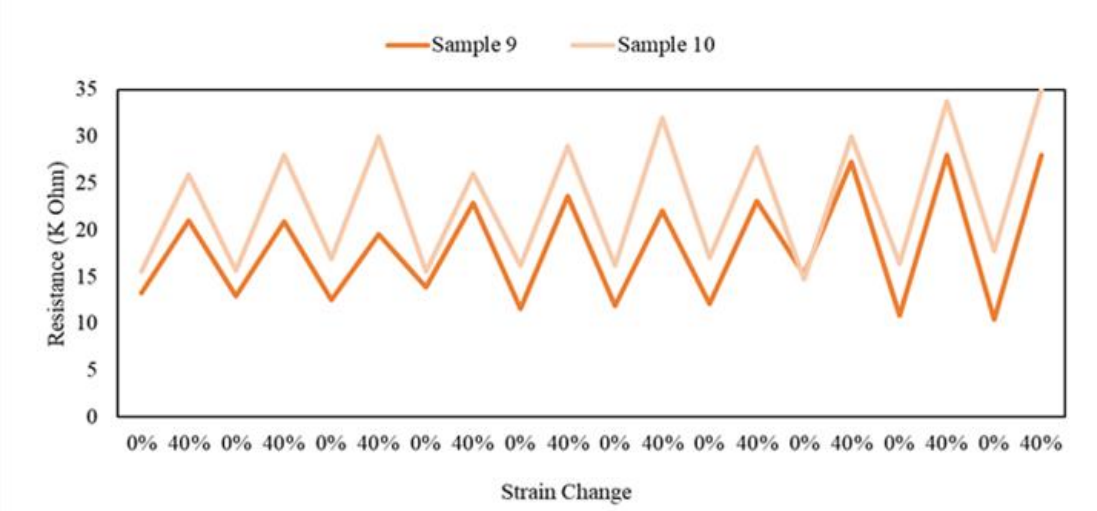

Figure 17. The resistance changes under the 40% cyclic strain change

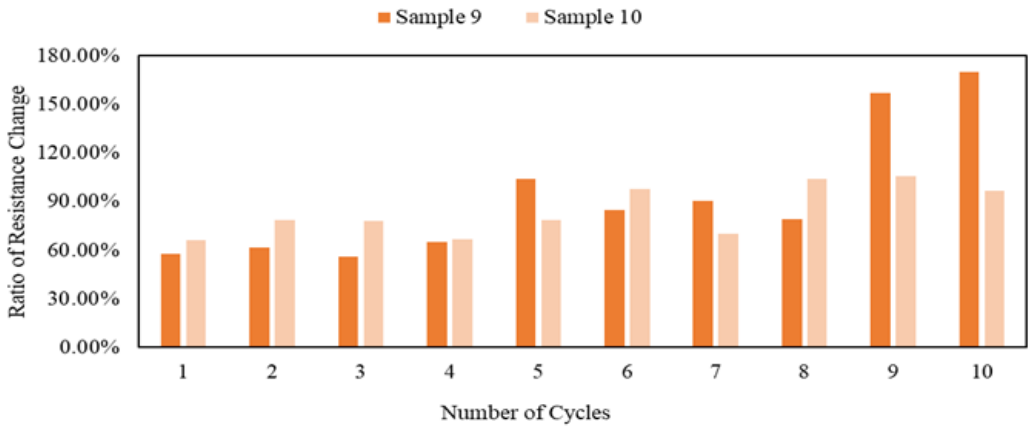

Figure 18. The $\Delta R/R$ changes under the 40% cyclic strain change

5. DISCUSSION

5.1 Limitations of This Research

In this study, the feasibility of fabricating stretchable piezo-resistive sensors with consistent fabrication quality and sensor electromechanical properties via FDM is investigated. Different methods of hardware modifications and filament preparation are tested to achieve a better fabrication of the designed sensors. Although satisfactory quality and electromechanical properties have been achieved, this research has certain limitations. At first, the number of replicates is 4 in the static tests and 5 in the cyclic tests. To obtain more comprehensive results, more replicated specimens are needed. Secondly, to scientifically understand why replicated samples have different electromechanical properties, more in-depth experimental characterizations, and analyses are needed on the microstructure and material properties using a higher resolution scanning electron microscope and differential scanning calorimetry. A microscopic study to see if the distribution of filler content in the polymer matrix is uniform or not is very important. Thirdly, the static testing results suggest that the sensors designed and fabricated in this research show a decent GF, a measure of sensitivity. But the sensitivity in some samples tends to be not enough for small strain changes. If the sensitivity is improved for small strain changes, samples printed in this way will have a good potential for manufacturing wearables. Fourthly, the cyclic testing results suggest that 30% strain works best in terms of both high and consistent output resistance. The reason why the 40% strain is yielding less resistance than the 30% strain needs to be investigated.

5.2 Academic Contribution

Previously, sensors were fabricated by FDM printer using conductive filament of 2 wt.% CNT/TPU, 3 wt.% CNT/TPU, 4 wt.% CNT/TPU, and 5 wt.% CNT/TPU. In this research, 7.5% CNT is mixed with TPU to prepare the conductive mixture and the filament. Secondly, the design

of the sensor is unique. Most of the papers have designed the conductive pattern such that the longer grid lines are along the longer side of the substrate and the shorter grid lines are along the shorter side of the substrate. In this research, a different design of the conductive pattern is printed. Every two conductive lines that are perpendicular to one another have almost an equal length. Thirdly, the preparation of the conductive mixture, the manufacturing of the filament, and printer settings are all important topics that are covered in length in this thesis (both hardware settings and process parameter settings). The experimentation method is difficult because of the addition of CNT in the TPU. This research goes into detail on the experiment so that future researchers can replicate, investigate and add to the process.

5.3 Next Step: Application in Wearable Sensors

The sensor is loaded with known values of strain. The corresponding values of resistance are determined for the applied strains to determine the GF. Once the GF is determined, the sensor is said to be calibrated [6]. Next, knowing the GF and the future measurements of resistance, the unknown strain can be determined which is the purpose of the sensor. If the GF is greater than 2, the sensor can be used in flexible sensor applications [9]. The performance of the sensor in real-life applications needs to be evaluated with sufficient collected data focusing on different perspectives including the reliability of the sensors, the comfort level of wearing the sensors, etc.

5.4 Future Research

The electromechanical properties of the stretchable piezo-resistive sensors (sensitivity both in static and dynamic testing) will be further attempted to be improved from various perspectives such as the conductive layer design (e.g., pattern and width), the sensor design, and the material design (e.g., changing the percentage of CNT and mixing other additives). To further facilitate the application of wearable sensors, smaller strain changes (such as 10%, and 5%) will be explored in

the dynamic testing to investigate if the printed piezo-resistive sensors are sensitive to small strain changes that are likely to happen with human body movements.

REFERENCES

[1] Ford S, Despeisse M. Additive manufacturing and sustainability: an exploratory study of the advantages and challenges. J Clean Prod 2016;137:1573–87. https://doi.org/10.1016/j.jclepro.2016.04.150.

[2] Pereira T, Kennedy J V., Potgieter J. A comparison of traditional manufacturing vs additive manufacturing, the best method for the job. Procedia Manuf 2019;30:11–8. https://doi.org/10.1016/j.promfg.2019.02.003.

[3] Wang J, Dommati H, Hsieh S. Review of additive manufacturing methods for high-performance ceramic materials 2019:2627–47.

[4] Ngo TD, Kashani A, Imbalzano G, Nguyen KTQ, Hui D. Additive manufacturing (3D printing): A review of materials, methods, applications and challenges. Compos Part B Eng 2018;143:172–96. https://doi.org/https://doi.org/10.1016/j.compositesb.2018.02.012.

[5] What is Additive Manufacturing? - The Future of 3D Printing n.d.

[6] Munasinghe N, Woods M, Miles L, Paul G. 3-D Printed Strain Sensor for Structural Health Monitoring. Proc IEEE 2019 9th Int Conf Cybern Intell Syst Robot Autom Mechatronics, CIS RAM 2019 2019:275–80. https://doi.org/10.1109/CIS-RAM47153.2019.9095826.

[7] Al Amin MAU, Yang Y, Kobir MH, Di L. Experimental Study of Microscopic Morphology and Material Property for Recycled Polyamide 12 Powder in Selective Laser Sintering 2022. https://doi.org/10.1115/MSEC2022-85618.

[8] Understanding Additive Manufacturing Hazards n.d. https://www.colden.com/manufacturing-hazards/.

[9] Kouchakzadeh S, Narooei K. Simulation of piezoresistance and deformation behavior of a

flexible 3D printed sensor considering the nonlinear mechanical behavior of materials. Sensors Actuators A Phys 2021;332:113214. https://doi.org/10.1016/j.sna.2021.113214.

[10] Newman ST, Zhu Z, Dhokia V, Shokrani A. Process planning for additive and subtractive manufacturing technologies. CIRP Ann 2015;64:467–70. https://doi.org/https://doi.org/10.1016/j.cirp.2015.04.109.

[11] Top 3 ways 3D Printing is transforming aircraft interiors n.d. https://www.stratasys.com/en/stratasysdirect/resources/articles/3d-printing-transforming-aircraft-interiors/.

[12] 10 exciting examples of 3D prinitng in the automotive industry in 2021 n.d. https://amfg.ai/2019/05/28/7-exciting-examples-of-3d-printing-in-the-automotive-industry/.

[13] 3 ways 3D Printing is revolutionizing health care n.d. https://www.aha.org/aha-center-health-innovation-market-scan/2022-06-07-3-ways-3d-printing-revolutionizing-health-care.

[14] 10 exciting ways 3D Printing is being used in consumer goods industry n.d. https://amfg.ai/2019/03/12/10-exciting-ways-3d-printing-is-being-used-in-the-consumer-goods-industry/.

[15] Dhinesh SK, Senthil Kumar KL. A Review on 3D Printed Sensors. IOP Conf Ser Mater Sci Eng 2020;764:0–7. https://doi.org/10.1088/1757-899X/764/1/012055.

[16] Mahale RS, Vasanth S, Krishna H, Chikkegouda SP, Rajendrachari S, Patil A, et al. Sensor-based additive manufacturing technologies. Biointerface Res Appl Chem 2022;12:3513–21. https://doi.org/10.33263/BRIAC123.35133521.

[17] Liu C, Huang N, Xu F, Tong J, Chen Z, Gui X, et al. 3D Printing Technologies for

Flexible Tactile Sensors toward Wearable Electronics and Electronic Skin. Polym 2018;10. https://doi.org/10.3390/polym10060629.

[18] Yu R, Xia T, Wu B, Yuan J, Ma L, Cheng GJ, et al. Highly Sensitive Flexible Piezoresistive Sensor with 3D Conductive Network. ACS Appl Mater Interfaces 2020;12:35291–9. https://doi.org/10.1021/acsami.0c09552.

[19] Yamada T, Hayamizu Y, Yamamoto Y, Yomogida Y, Izadi-Najafabadi A, Futaba DN, et al. A stretchable carbon nanotube strain sensor for human-motion detection. Nat Nanotechnol 2011;6:296–301. https://doi.org/10.1038/nnano.2011.36.

[20] Lou Z, Chen S, Wang L, Jiang K, Shen G. An ultra-sensitive and rapid response speed graphene pressure sensors for electronic skin and health monitoring. Nano Energy 2016;23:7–14. https://doi.org/https://doi.org/10.1016/j.nanoen.2016.02.053.

[21] Alsharari M, Chen B, Shu W. 3D Printing of Highly Stretchable and Sensitive Strain Sensors Using Graphene Based Composites. Proc 2018;2. https://doi.org/10.3390/proceedings2130792.

[22] Chun S, Kim Y, Jin H, Choi E, Lee S-B, Park W. A graphene force sensor with pressure-amplifying structure. Carbon N Y 2014;78:601–8. https://doi.org/https://doi.org/10.1016/j.carbon.2014.07.051.

[23] Obitayo W, Liu T. A review: Carbon nanotube-based piezoresistive strain sensors. J Sensors 2012;2012. https://doi.org/10.1155/2012/652438.

[24] Christ JF, Aliheidari N, Ameli A, Pötschke P. 3D printed highly elastic strain sensors of multiwalled carbon nanotube/thermoplastic polyurethane nanocomposites. Mater Des 2017;131:394–401. https://doi.org/10.1016/j.matdes.2017.06.011.

[25] Christ JF, Aliheidari N, Pötschke P, Ameli A. Bidirectional and Stretchable Piezoresistive

Sensors Enabled by Multimaterial 3D Printing of Carbon Nanotube/Thermoplastic Polyurethane Nanocomposites. Polym 2019;11. https://doi.org/10.3390/polym11010011.

[26] Gong S, Schwalb W, Wang Y, Chen Y, Tang Y, Si J, et al. A wearable and highly sensitive pressure sensor with ultrathin gold nanowires. Nat Commun 2014;5:1–8. https://doi.org/10.1038/ncomms4132.

[27] Li Z, Feng D, Li B, Xie D, Mei Y, Zeng T. Fabrication and Properties of Thermoplastic Polyurethane/Silver Parts via Fused Deposition Modeling for Electromagnetic Interference Shielding and Wearable Sensors. Adv Eng Mater 2021;2101392:1–10. https://doi.org/10.1002/adem.202101392.

[28] Lee J, Kim S, Lee J, Yang D, Park BC, Ryu S, et al. A stretchable strain sensor based on a metal nanoparticle thin film for human motion detection. Nanoscale 2014;6:11932–9. https://doi.org/10.1039/c4nr03295k.

[29] 3D Printing and Design, Clone 3D Print and Production n.d. https://www.clone3d.co.nz/printer-and-plastic/.

[30] Vu CC, Nguyen TT, Kim S, Kim J. Effects of 3D Printing-Line Directions for Stretchable Sensor Performances. Mater 2021;14. https://doi.org/10.3390/ma14071791.

[31] Mousavi S, Howard D, Wu S, Wang C. An Ultrasensitive 3D Printed Tactile Sensor for Soft Robotics 2018.

[32] Lanzotti A, Grasso M, Staiano G, Martorelli M. The impact of process parameters on mechanical properties of parts fabricated in PLA with an open-source 3-D printer. Rapid Prototyp J 2015;21:604–17. https://doi.org/10.1108/RPJ-09-2014-0135.

[33] Moorthi A, Narakathu BB, Reddy ASG, Eshkeiti A, Bohra H, Atashbar MZ. A novel flexible strain gauge sensor fabricated using screen printing. Proc Int Conf Sens Technol

ICST 2012:765–8. https://doi.org/10.1109/ICSensT.2012.6461780.

[34] Muth JT, Vogt DM, Truby RL, Mengüç Y, Kolesky DB, Wood RJ, et al. Embedded 3D printing of strain sensors within highly stretchable elastomers. Adv Mater 2014;26:6307–12. https://doi.org/10.1002/adma.201400334.

[35] Valentine AD, Busbee TA, Boley JW, Raney JR, Chortos A, Kotikian A, et al. Hybrid 3D Printing of Soft Electronics. Adv Mater 2017;29. https://doi.org/10.1002/adma.201703817.

[36] Li X. HHS Public Access. Physiol Behav 2016;176:139–48. https://doi.org/10.1002/adma.201701218.3D.

[37] Pellets, LNS Technologies n.d. https://www.techkits.com/collections/pellets/.

[38] White TPU melt adhesive powder for heat transfer printing n.d. https://www.stsinks.com/?s=TPU&post_type=product.

[39] Carbon nanotube, single-walled, SWCNT, SWNT n.d. https://www.sigmaaldrich.com/US/en/product/aldrich/805033.

[40] Mora A, Verma P, Kumar S. Electrical conductivity of CNT/polymer composites: 3D printing, measurements and modeling. Compos Part B Eng 2020;183:107600. https://doi.org/10.1016/j.compositesb.2019.107600.

[41] Moheimani R, Aliahmad N, Aliheidari N, Agarwal M, Dalir H. Thermoplastic polyurethane flexible capacitive proximity sensor reinforced by CNTs for applications in the creative industries. Sci Rep 2021;11:1–12. https://doi.org/10.1038/s41598-020-80071-0.

[42] Geckeler KE, Premkumar T. Carbon nanotubes: Are they dispersed or dissolved in liquids? Nanoscale Res Lett 2011;6:136. https://doi.org/10.1186/1556-276X-6-136.

[43] Wah LF, Liu WW, Hashim U, Lai CW. The Effect of Chemical Solutions (Isopropyl Alcohol, Dichloromethane, Acetone and Triton X-100) on the Dispersion of Single-Walled Carbon Nanotubes. Adv Mater Res 2015;1109:113–7. https://doi.org/10.4028/www.scientific.net/amr.1109.113.

[44] Kim NP. 3D-printed conductive carbon-infused thermoplastic polyurethane. Polymers (Basel) 2020;12. https://doi.org/10.3390/POLYM12061224.

[45] Souri H, Banerjee H, Jusufi A, Radacsi N, Stokes AA, Park I, et al. Wearable and Stretchable Strain Sensors: Materials, Sensing Mechanisms, and Applications. Adv Intell Syst 2020;2:2000039. https://doi.org/10.1002/aisy.202000039.

[46] Shin S, Ko B, So H. Structural effects of 3D printing resolution on the gauge factor of microcrack-based strain gauges for health care monitoring. Microsystems Nanoeng 2022;8. https://doi.org/10.1038/s41378-021-00347-x.

[47] Cortés A, Sánchez-Romate XF, Jiménez-Suárez A, Campo M, Ureña A, Prolongo SG. Mechanical and Strain-Sensing Capabilities of Carbon Nanotube Reinforced Composites by Digital Light Processing 3D Printing Technology. Polymers (Basel) 2020;12. https://doi.org/10.3390/polym12040975.